Rotational relaxation of a molecule trapped in a three-dimensional crystal. III. Environmental effects and relaxation channels

V. Delgado, J. Breton, E. Alvira, and J. Plata
Departamento de Fisica Fundamental y Experimental, Universidad de La Laguna, Tenerife, Spain
C. Girardet[a)]
Département de Physique, Université de Besançon, La Bouloie, 25030 Besançon Cedex, France

(Received 13 April 1989; accepted 22 June 1989)

The stochastic classical trajectory method is used to calculate the energy relaxation of a highly excited diatomic rotor trapped in rare gas crystal at $T = 20$ K. The friction kernels, which appear in the generalized Langevin equations characterizing the motions of the molecule and of nearest neighbor crystal atoms, are expressed in terms of the interaction potentials. The influence of the surrounding crystal on the relaxation mechanism and the efficiency of the various dissipation channels are analyzed by changing the rare gas species and by artificially switching off some channels. Within the limits of the model (classical two-dimensional rotation of the diatomic molecule, coupled on the one hand to a restricted number of first shell atoms themselves coupled to the bulk crystal and on the other hand to the other first shell atoms considered as pertaining to the bath), the results of the calculations show that, in the present case, rotational relaxation is a rapid process, over the picosecond scale, and that the local mode connected to the motions of the molecular center of mass plays a major role in the mechanism. This local mode is responsible, at short times $t \leqslant 0.5$ ps, for the relaxation of 95%, 75%, and 60% of the rotational energy excess in Ar, Kr, and Xe crystals, respectively. The remaining energy is then dissipated over longer times via the local mode or directly towards the crystal modes. A striking energy saturation phenomenon of the local mode is exhibited in xenon crystal.

I. INTRODUCTION

The study of nonradiative relaxation processes of molecular systems in the condensed phase provides noticeable information on the interaction potentials and on the dynamics of these systems. Phase and energy relaxations of impurity molecules trapped in matrices have been extensively investigated[1] from an experimental point of view, more specially for diatomic[2] and symmetric top species.[3]

To overcome the difficulty connected to a realistic description of the dynamic couplings between the molecule and the crystal, the theoretical approaches generally assume that only a dominant process, among all the possibilities, contributes to the relaxation mechanism. The vibrational energy relaxation of molecules trapped in matrices is usually considered as a multiphonon process.[4] The molecular vibrational quantum is dissipated over the phonons of the lattice unaffected by the presence of the molecule, but experiments on hydrogenated molecules[1-3] have suggested that orientational and translational local modes of the molecule can play a major role as energy acceptors. So, quantum models have been developed[5-9] to include the influence of these local modes in the relaxation. These models are yet either very simple and qualitative or accurate and extremely complicated. Moreover, revisited interpretations[10] of the vibrational relaxation of larger molecules (CH_3F) lead to the conclusion that all the relaxation channels (multiphonon, pure local modes and mixed ones) contribute in a similar way to the energy dissipation.

From these features, it thus appears as essential to get more information on the manner the local modes influence the dynamic coupling between the energy donor and the ultimate acceptor. Since the molecular orientational modes appear to be privileged quasiresonant modes for the vibrational quantum, the study of the depopulation of highly excited rotational levels of a molecule is a crucial step in the interpretation of the relaxation mechanism of the vibrational energy.

We use here a quasiclassical description for the dynamics of the trapped molecule, developed in previous papers (I[11] and II[12]). The crystal dynamics is described first by the motions of a reduced number of nearest-neighbor atoms and second by stochastic terms characterizing the crystal influence, included in the classical equations of motion of the molecule and of the nearest-neighbor atoms. The generalized Langevin equations thus obtained for the reduced system are then solved using a numerical integration, within the framework of the stochastic classical trajectory method.

A classical description of typically quantal phenomena frequently becomes a powerful tool for the interpretation of complicated molecular systems. For these systems, complete quantum mechanical calculations become untractable, and simulations[11-15] are generally pertinent alternatives for describing atomic motions and time-dependent molecular processes. Such an alternative appears in fact much more accurate than expected *a priori* because the statistical average over the dynamics of the system hides the quantum behavior. Consequently, the calculated macroscopic observables connected to the relaxation mechanisms exhibit, in the classical approach, the main aspects of the measured ones. For low temperature crystals, the classical approximation

[a)] To whom correspondence should be addressed.

 0021-9606/89/204625-11$02.10

must, however, be slightly corrected. In order to take into account the zero point motions, it is necessary to introduce, as discussed in Ref. 13(c), an effective quasiclassical temperature, defined as the equivalent temperature needed to produce the quantum average energy of the bath oscillators.

In this paper, we study the rotational relaxation of the typical molecule CO trapped in argon, krypton, and xenon crystals at $T = 20$ K. The molecule is assumed to be highly excited, with an equivalent quantum energy corresponding to the rotational quantum number $j = 30$. Such a value corresponds approximately to the energy of the vibrational quantum $v = 1 \rightarrow v = 0$. Although it is now known[2] that the vibrational relaxation of CO is a radiative process with energy migration inside the rare gas crystal, this diatomic rotor with a relatively large moment of inertia is appropriate for a classical approach and helps as a model for other trapped species. The present study is also a complement of previous results obtained[12] for the relaxation of the same trapped molecule, but with a much smaller rotational energy ($j \leqslant 10$).

The main aspects of the stochastic trajectory approach are presented in Sec. II; more details can be found in papers I and II. The numerical background necessary to the calculation of the various energy observables is given in Sec. III. The results are presented in Sec. IV and the environmental effects on the relaxation mechanisms are studied by changing the matrix. The efficiency of the various relaxation channels and, more particularly, the importance of the local modes as intermediate energy acceptors is analyzed in Sec. V, by considering each relaxation channel in a separated way. The application of the method to another physical systems is discussed in Sec. VI.

II. THE MODEL

The formal approach and the methodology needed for the interpretation of the energy relaxation are explained in paper I. The total system "molecule–crystal" is separated into three parts:

(i) the substitutionally trapped molecule which undergoes planar rotation and vibrations in the vicinity of the equilibrium crystal site;

(ii) the primary system formed by four crystal atoms which are nearest neighbors of the molecule and located in the plane of the molecular rotation (these atoms vibrate around the equilibrium positions of the distorted crystal);

(iii) the remaining crystal, which contains all the other degrees of freedom in three dimensions, is referenced as the bath.

Figure 1 represents the molecule and the primary system. The interactions among the three partners "molecule-primary system–bath" are described by pairwise atom–atom 6-exp potentials. Each partner interacts directly with the two others and can thus dissipate its energy on all the modes of the other partners. We then assume that the bath motions are harmonic and use Laplace transform technics to eliminate the explicit dependence of the bath coordinates in the equations of motion tied to the molecule and to the primary system. The 11 remaining equations of motions connected to the rotation θ and vibration $\mathbf{u}_0$ of the molecule center of mass (c.m.) and to the vibrations $\mathbf{u}_p$ ($p = 1,...,4$) of the four

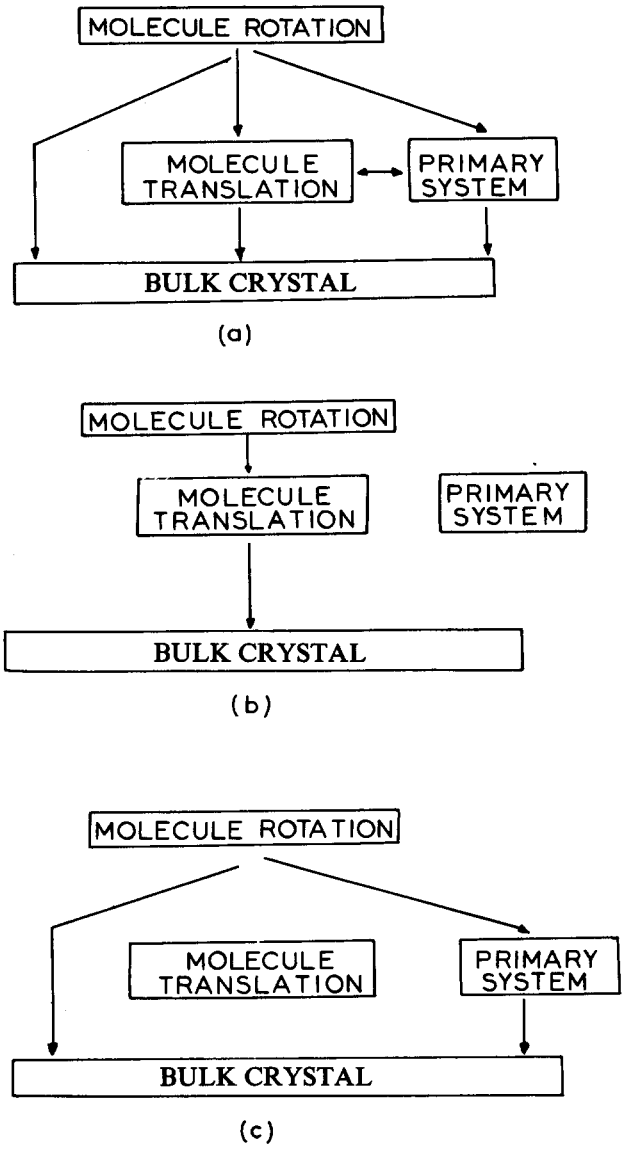

FIG. 1. Various partners and relaxation channels (arrows). (a) The general case; (b) relaxation via the translational mode of the molecule, only; (c) direct relaxation on the crystal.

atoms of the primary system are written, after algebraic manipulations, as[11]

$$\begin{aligned}
\ddot{\theta}(t) &= I^{-1}F_\theta + \bar{\Lambda}_\theta(0)(\theta(t) - \theta_0) - \beta_\theta\dot{\theta}(t) + N_\theta(t), \\
\ddot{\mathbf{u}}_0(t) &= M_0^{-1}\mathbf{F}_0 + \bar{\Lambda}_0(0)\mathbf{u}_0(t) - \bar{\beta}_0\dot{\mathbf{u}}_0(t) + \mathbf{N}_0(t), \qquad (1) \\
\ddot{\mathbf{u}}_p(t) &= M^{-1}\mathbf{F}_p + \bar{\Lambda}_p(0)\mathbf{u}_p(t) - \bar{\beta}_p\dot{\mathbf{u}}_p(t) + \mathbf{N}_p(t).
\end{aligned}$$

Equations (1) are generalized Langevin equations. They contain the torque F_θ and the forces $\mathbf{F}$ experienced by the molecule with moment of inertia I and mass M_0 and by the pth atom of the primary system with mass M. These forces characterize both the instantaneous influence of the other partner and the effect of the static bath. $\Lambda_\theta(0)$ and $\bar{\Lambda}(0)$ are (1×1) and (2×2) tensors, respectively, which describe the renormalization of the motions of the molecule and of the primary system by the bath motions. The friction coefficients β_θ and $\bar{\beta}$ are responsible for the energy dissipation of the rotational or translational modes of the molecule and of the vibrational modes of the primary system directly

towards the bath. These coefficients are also (1×1) and (2×2) tensors, respectively. The remaining torque $N_\theta(t)$ and forces $\mathbf{N}(t)$ in Eqs. (1) are the random forces due to the influence of the thermal motion of the bath modes on the primary system and on the molecule. The temperature T of the crystal is accurately introduced through the second fluctuation–dissipation theorem relating the random force correlations and the friction kernels, as[11]

$$\langle N_\epsilon(0)N_\epsilon(t)\rangle = 2k_B T M_\epsilon^{-1}\beta_\epsilon\delta(t) \qquad (2)$$

with $M_\epsilon = I$, M_0 or M according to $\epsilon = \theta$, 0 or P. The delta function comes from the fact that the Markovian approximation has been used. $\Lambda_\epsilon(0)$, β_ϵ, and N_ϵ are then given in terms of tensors T_ϵ which characterize the intensity of the coupling between the motions of the "molecule + primary system" and the bath, as

$$\Lambda_\epsilon(0) = \Omega T_\epsilon, \quad \beta_\epsilon = \Gamma T_\epsilon. \qquad (3)$$

Ω and Γ are constants which depend only on the dynamical characteristics of the crystal and they are easily evaluated[11–14] from the knowledge of the phonon density of states of the perfect crystal. The tensors T_ϵ are proportional[11] to the ratio of the inertia elements M/M_ϵ and to the coupling force constants between the ϵ motion and the bath motions. These force constants are calculated from the expression of the interaction potential. Thus, the behavior of $\Lambda_\epsilon(0)$, β_ϵ, and $N_\epsilon(t)$ ($\epsilon = \theta$ and 0) is very sensitive to changes of the ratios M/I or M/M_0 and of the corresponding dynamical couplings. These couplings characterize the direct dissipation efficiency of the rotational or translational energy of the molecule towards the bath. Since the local modes are coupled together and to the crystal, all the relaxation channels are thus considered in our model.

The present dynamical model can be compared to those reported in the literature.[13–15] More particularly, it does not use all the ingredients of the more complete molecular time scale generalized Langevin theory (MTGLE) within the framework of the chain equation formalism.[15] According to this approach, the energy of the donor system is dissipated into the bath via stepwise flow through successive atomic shells around the donor, whereas the conventional Langevin method considers the bath as a continuum bulk. In the present paper, the first crystal shell is restricted to four atoms assumed to be more efficiently coupled to the diatomic rotor than the eight other atoms of this shell. These eight atoms and the other shells play the role of a bulk bath for the exact dynamics of the molecule and its four privileged neighbors coupled to the Langevin bath. Our model appears as an intermediate between the MTGLE truncated at the first chain equation step and the conventional Langevin method, in the sense that it allows us to consider possible resonances and feedback energy flow between the molecule and the four atoms, but it prevents such phenomena between the four atoms and the surrounding crystal.

TABLE II. Dynamic parameters for rare gas crystals.

X	a ω_D (cm^{-1})	b ω_0 (cm^{-1})	c Γ (ps^{-1})	c Ω (ps^{-2})
Ar	64	45	2.00	1.00
Kr	50	35	1.56	0.61
Xe	44.5	31	1.39	0.48

[a]Debye frequency from *Rare Gas Crystal*, edited by M. L. Klein and J. A. Venables (Academic, London, 1977), Vol. II.
[b]Vibrational frequency used to determine the equivalent temperature T_{QC}.
[c]Dynamic parameters used to calculate the frequency renormalizations and the friction terms; cf. paper I.

III. NUMERICAL BACKGROUND

The previous formalism is applied to the motion of a model molecule CO trapped in Ar, Kr, and Xe matrices at $T = 20$ K. The various parameters used in the 6-exp pairwise atom–atom potential and the dynamical characteristics of the three rare gas crystals are given in Tables I and II, respectively.

The equilibrium configuration for the distorted crystal due to the substitutional molecule is obtained with respect to the perfect crystal one by integrating Eqs. (1) at $T = 0$ K, as explained in the appendix of paper II. T_ϵ tensors are then calculated (cf. Table III) and the corresponding terms $\Lambda_\epsilon(0)$ and β_ϵ can be evaluated. The random forces defined

TABLE I. Potential parameters for the pairs CO–rare gas.

Pair	A (KJ mol^{-1} Å^6)	$B\times10^{-5}$ (KJ mol^{-1})	α (Å^{-1})	Footnote
Ar–Ar	6 554	3.27	3.305	a
C–Ar	3 379	3.12	3.493	a
O–Ar	2 737	3.28	3.706	a
Kr–Kr	11 443	2.75	3.033	b
C–Kr	4 466	2.85	3.348	c
O–Kr	3 660	3.00	3.545	c
Xe–Xe	27 726	7.29	2.921	b
C–Xe	7 085	4.66	3.273	c
O–Xe	5 927	4.90	3.455	c

[a]K. Mirsky, Chem. Phys. **46**, 445 (1980).
[b]J. O. Hirschfelder, C. F. Curtiss, and R. B. Bird, *Molecular Theory of Gases and Liquids* (Wiley, New York, 1967).
[c]These results have been obtained from a and b after applying the usual combination rules.

TABLE III. Tensors T.[a]

Matrix	T_1	T_2	T_3	T_4	T_0	T_θ
Argon XX	1	1	1	1	0.908	
ZZ	1	1	1	1	0.183	0.275
XZ	−0.072	0.072	−0.041	0.041	0.0	
Krypton XX	1	1	1	1	0.906	
ZZ	1	1	1	1	0.138	0.285
XZ	−0.196	0.196	−0.181	0.181	0.0	
Xenon XX	1	1	1	1	0.228	
ZZ	1	1	1	1	0.021	0.074
XZ	−0.353	0.353	−0.349	0.349	0.0	

[a]These results are for the well corresponding to $\theta_0 = \pi/2$; for the three remaining wells, equivalent results can be obtained from the symmetry rules of the crystal (cf. paper II).

by Eq. (2) are assumed to be white noise Gaussian random forces. The numerical treatment of the Dirac function in Eq. (2) is done according to the algorithm developed in Ref. 15. Thus the random forces are treated as Gaussian random variables characterized by the matrix autocorrelation functions

$$\langle N_\epsilon(0)N_\epsilon(0)\rangle = \frac{2k_BT}{M_\epsilon \Delta t}\beta_\epsilon, \tag{4}$$

where Δt is the numerical integration time step.

The equations of motion (1) have been solved by using a one-step integrator subroutine. The convergence has been tested first by vanishing the nonconservative terms in Eqs. (1) and verifying that the total energy remains constant, and second by considering all the terms in the equations of motion and using two different one-step integrator subroutines with the same path Δt. The value $\Delta t = 6.25\times 10^{-3}$ ps is sufficient to ensure an accuracy better than 0.5% on the locations and velocities of the molecule and of the primary system, inside the integration domain. As mentioned before, an effective quasiclassical temperature T_{QC} must be introduced in order to take into account the zero point motions of the crystal. The averages over the trajectories of the molecule and of the atoms of the primary systems are then obtained for initial conditions selected by a Monte Carlo sampling from a canonical thermal distribution at the temperature[13]

$$T_{QC} = \frac{\hbar\omega_0}{2k_B}\coth\frac{\hbar\omega_0}{k_BT}, \tag{5}$$

where ω_0 characterizes the vibrational frequency of the crystal atoms assumed to behave like 2D isotropic oscillators. The values of ω_0 for the rare gas crystals are given in Table II.

Numerical tests on the behavior of the random forces $\mathbf{N}_\epsilon(t)$ have been performed by integrating Eqs. (1) for the CO/Ar crystal system in thermal equilibrium at $T = 20$ K. The total energy and the energies of the molecule and of the primary system have been calculated for a time integration interval equal to 9 ps, after averaging over 1200 trajectories. It has been verified that all these energies remain constant with time and are equal to the values obtained from a Monte Carlo sampling calculation.

Then, the rotational excitation of CO, at $t = 0$, is introduced in the equations of motion by replacing the thermal rotational kinetic energy of the molecule by its value obtained for $j = 30$. The rotational relaxation mechanism is first studied by considering all the dissipative channels, as schematized in Fig. 1(a). Environmental effects are analyzed for the three rare gas crystals Ar, Kr, and Xe. The relative contributions of the various dissipative channels are then calculated by assuming the rotational energy is entirely transferred to the crystal via the motion of the molecular c.m. [Fig. 1(b)] or directly transferred to the primary system and to the bulk crystal [Fig. 1(c)].

In the first case [Fig. 1(b)], the dynamical coupling between the molecule and the primary system is switched off by fixing the four p atoms at their equilibrium configuration; and the direct coupling between the CO rotation and the bulk crystal is taken to be zero ($\beta_\theta = 0$). Such a numerical procedure has nevertheless a drawback. Indeed, since the atoms of the primary system do not move, the energy relaxation from the local c.m. mode to these atoms is forbidden. So, we can expect that the dissipative ability of this local mode towards the remaining energy acceptors (the bulk crystal) is appreciably reduced. Unfortunately, there is not another simple way for monitoring the rotational energy flux exclusively through the local mode, without altering in a drastic manner the equations of motion.

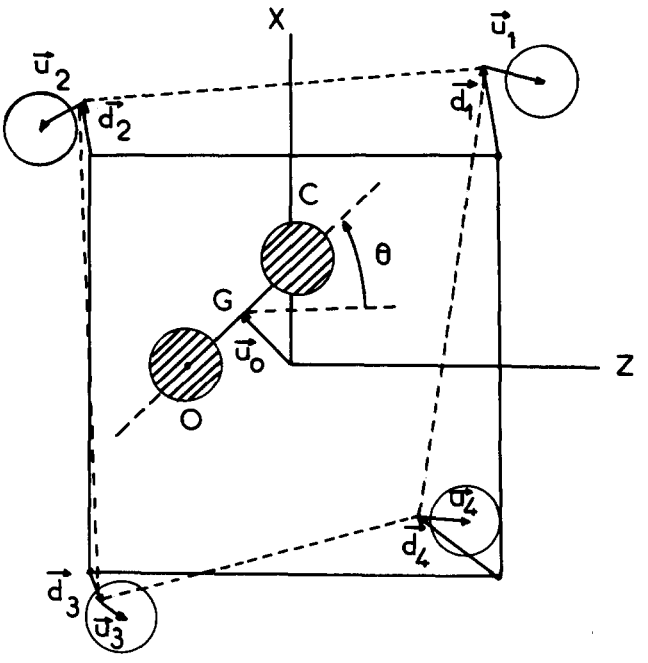

FIG. 2. Instantaneous configurations of the CO molecule and of the primary system. The square (solid lines) and deformed square (dashed lines) connect the equilibrium locations of the atoms in the perfect and doped crystals, respectively. d is the distortion vector, whereas u and θ are dynamical variables.

In the second case [Fig. 1(c)], the molecule c.m. is assumed to be fixed at its equilibrium position and therefore all the dynamical couplings, implying this local mode, vanish.

For the three situations of Fig. 1, 800 trajectories are considered for time intervals equal to 3 ps which lead to the computation of the probability distribution function $P(j,t)$ for the rotational quantum number j.[16] The mean rotational energy of the molecule is then defined, in the quasiclassical approach, as

$$\langle E_{rot}(t)\rangle = \sum_{j=0}^{\infty} B(j+1)jP(j,t), \tag{6}$$

where B characterizes the CO rotational constant ($B = 1.93$ cm^{-1}). The other mean energies $\langle E_{c.m.}(t)\rangle$ and $\langle E_{at}(t)\rangle$ for the molecular c.m. and the primary system are strictly classical quantities.

IV. ENVIRONMENTAL EFFECTS ON THE ENERGY RELAXATION PROCESS

A. Argon crystal

Figures 3(a) and 3(b) exhibit the time evolution of the probability distribution function $P(j,t)$ and of the mean rotational energy $\langle E_{rot}(t)\rangle$ of the molecule, respectively. Figure 3(b) shows that 95% of the rotational energy has been

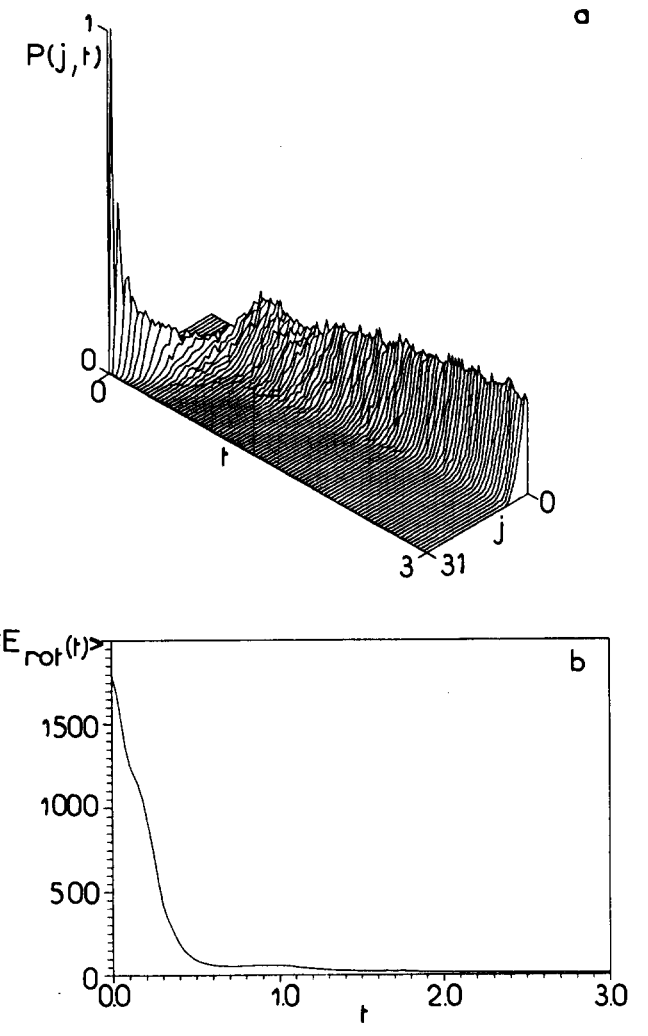

FIG. 3. Rotational relaxation energy for CO trapped in argon crystal. (a) The probability distribution function $P(j,t)$ for the rotational quantum number j (time t in ps); (b) mean rotational energy vs time (energy in cm^{-1}).

released after a time $t = 0.5$ ps; the remaining 5% is then dissipated over a time of about 3 ps. The distribution function in Fig. 3(a) is sharp; this indicates a more probable j value at each time which corresponds, in a quantum scheme, to a level-to-level relaxation mechanism. After a rapid drift of the probability maxima with time from $j = 30$ to $j \simeq 10$, these maxima tend to slowly evolve down to the lower values of j, with a distribution shape which looks like the equilibrium Maxwell–Boltzmann distribution. At very short time, the probability for finding the molecule on the excited rotational level $j = 31$ does not vanish ($P \simeq 0.38\%$); indeed the absorption of two phonons by the molecule with energy $2 \times 60\ cm^{-1}$ nearly equal to the level spacing though highly unprobable, at low temperature, is nevertheless possible.

The probability distribution function $P(E,t)$ for the total energy E of the reduced system "molecule + primary system" is shown in Fig. 4 as a function of E and t. In an inset appears the corresponding mean energy $\langle E(t) \rangle$, which monotonously decreases with time; 2.5 ps are required to dissipate the initial energy towards the bulk crystal. The distribution function is here again concentrated around the most

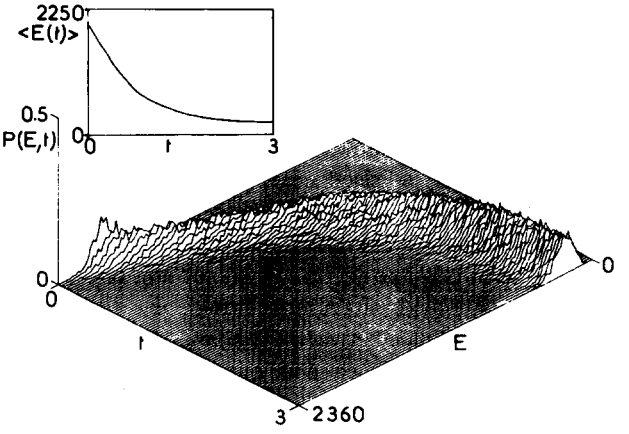

FIG. 4. Behavior of the energy of the system "molecule + primary system" vs time. The probability distribution function $P(E,t)$ and corresponding mean energy $\langle E(t) \rangle$ for CO trapped in argon (t in ps and E in cm^{-1}).

probable values at each time. The fact that the relaxation time for the energy E appears to be five times longer than the time characterizing the rotational energy dissipation suggests a participation of intermediate local modes. This feature will be analyzed in Sec. V A.

Figures 5(a) and 5(b) exhibit the behavior of the probability distribution functions $P(E_{c.m.},t)$ and $P(E_{at},t)$ for the

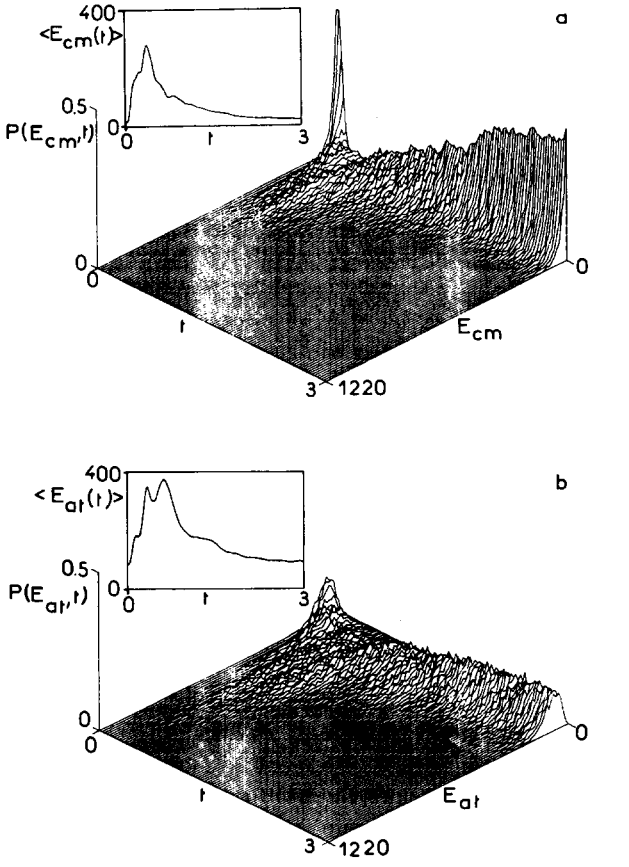

FIG. 5. Rotational relaxation for CO trapped in argon crystal (a) Energy of the local translational mode vs time. The probability distribution function $P(E_{c.m.},t)$ and mean energy $\langle E_{c.m.}(t) \rangle$. (b) Energy of the primary system modes vs time. The probability distribution function $E(P_{at},t,)$ and mean energy $\langle E_{at}(t) \rangle$.

energies of the molecular c.m. and of the primary system. The corresponding mean energies are given in insets. The comparison with curves of Figs. 3 shows that the rotational energy is dissipated, at very short times on the translational molecular mode which has its maximum excitation when the rotational mode has released nearly all its energy (i.e., at $t \simeq 0.5$ ps). Indeed, the probability distribution function for the local mode energy exhibits a sharp peak for $t \simeq 0.5$ ps which corresponds to the excitation maximum. In contrast, the primary system exhibits a more broadened distribution function. The difference between the shapes of the distributions at short time is a consequence of the local nature of the translational molecular mode and of the collective character of the primary system modes.

The relaxation process of the local mode is relatively rapid since the equilibrium distribution is obtained for times around 2 ps. The fact that this distribution remains concentrated around more probable energy values can be interpreted as the inability for the molecular c.m. to store and dissipate any energy quantity. This energy selectivity is a characteristic of the local nature of the translational motion. In contrast, the distribution function connected to the primary system energy is broadened and the energy dissipation towards the bulk crystal is much less efficient in that case. This is a consequence of the, at least partial, collective nature of the motions of the primary system. Eight modes with frequencies located inside the bulk crystal phonon band (instead of two with localized frequency for the molecular c.m.) can accept energy. Note also the occurrence of a second peak in the curve $\langle E_{at}(t) \rangle$, which is probably due to the deexcitation of the local mode towards the primary system.

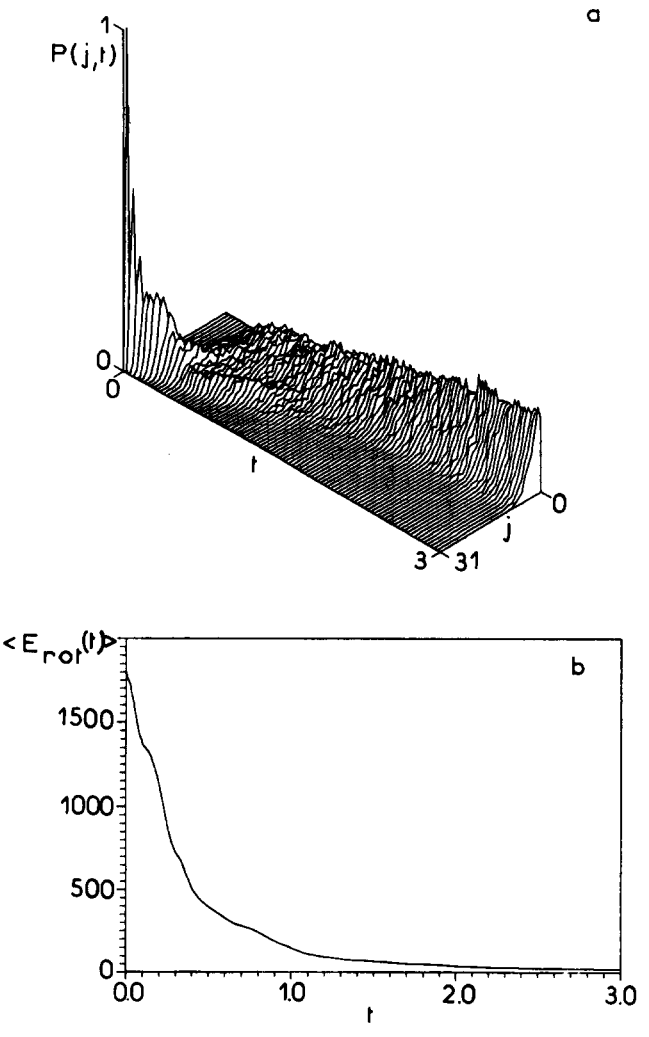

FIG. 6. Rotational relaxation energy for CO trapped in krypton crystal (the same as Fig. 3).

B. Krypton crystal

The probability distribution function $P(j,t)$ for the rotational number and the mean rotational energy $\langle E_{rot}(t) \rangle$ for CO trapped in krypton crystal are represented in Figs. 6(a) and 6(b), respectively. At short times ($t \leqslant 0.4$ ps) there is no significant difference with the results obtained with argon; at longer time, the relaxation rate decreases significantly since at $t = 1$ ps, the mean energy $\langle E_{rot}(t) \rangle$ of the molecule is still equal to 150 cm^{-1} in Kr instead of 70 cm^{-1} in Ar. The distribution function exhibits in the time interval (0.4–1.5 ps) a broadened structure leading to the occurrence of intermediate values of j ($20 < j < 10$) with a noticeable probability. A second curve of probability maxima appears with a less efficient dissipation mechanism since the rotational energy can remain appreciably large over 1 ps. This second process, which does not occur in argon, suggests the superimposition of two relaxation channels.

The distribution functions $P(E,t)$, $P(E_{c.m.},t)$, and $P(E_{at},t)$ drawn in Figs. 7, 8(a), and 8(b), respectively, do not exhibit significant differences with those given for argon; the only difference is a general broadening of the distributions which reveals a trend for a less efficient energy dissipation in krypton. The insets of these figures show that the mean energy of the reduced system (molecule + primary system) monotonously decreases, but with a slower rate. Moreover, a shoulder for $t \simeq 1.1$ ps clearly appears in the curve of $\langle E_{c.m.}(t) \rangle$, which is connected to a lesser dissipation efficiency for the local mode. This feature is also evidenced in the curve $\langle E_{at}(t) \rangle$ for the primary system since the energy remains equal to about 250 cm^{-1} over 1 ps and then decreases slowly.

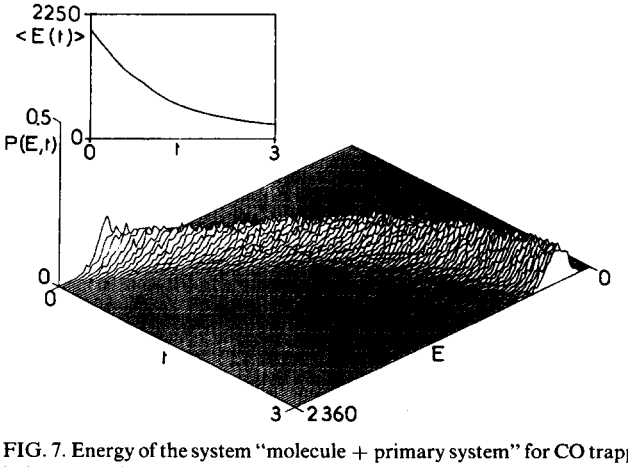

FIG. 7. Energy of the system "molecule + primary system" for CO trapped in krypton (the same as Fig. 4).

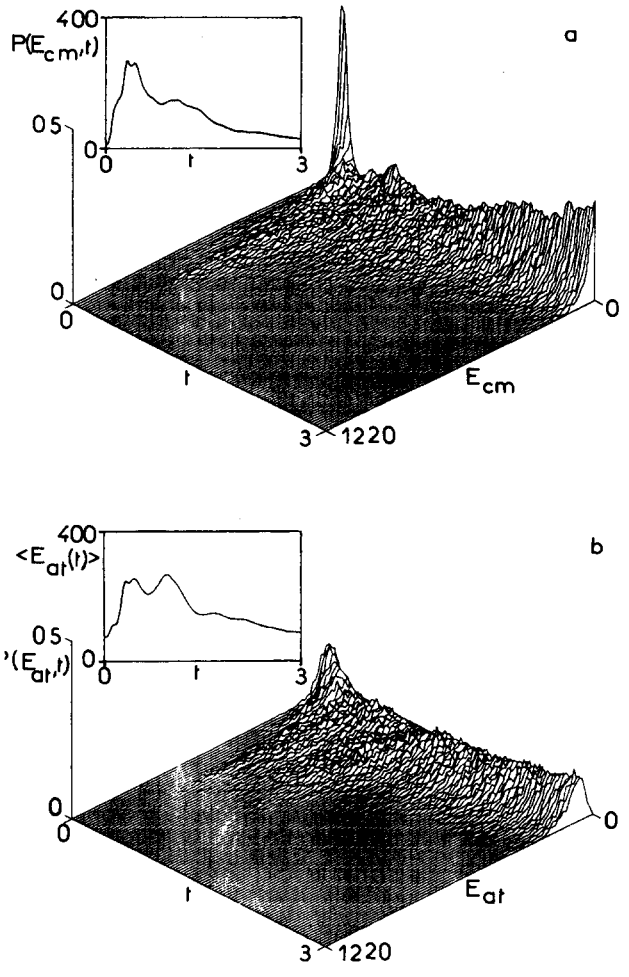

FIG. 8. Rotational relaxation for CO trapped in krypton crystal. (a) Energy (cm^{-1}) of the local translational mode vs time (ps); (b) energy (cm^{-1}) of the primary system modes vs time (ps).

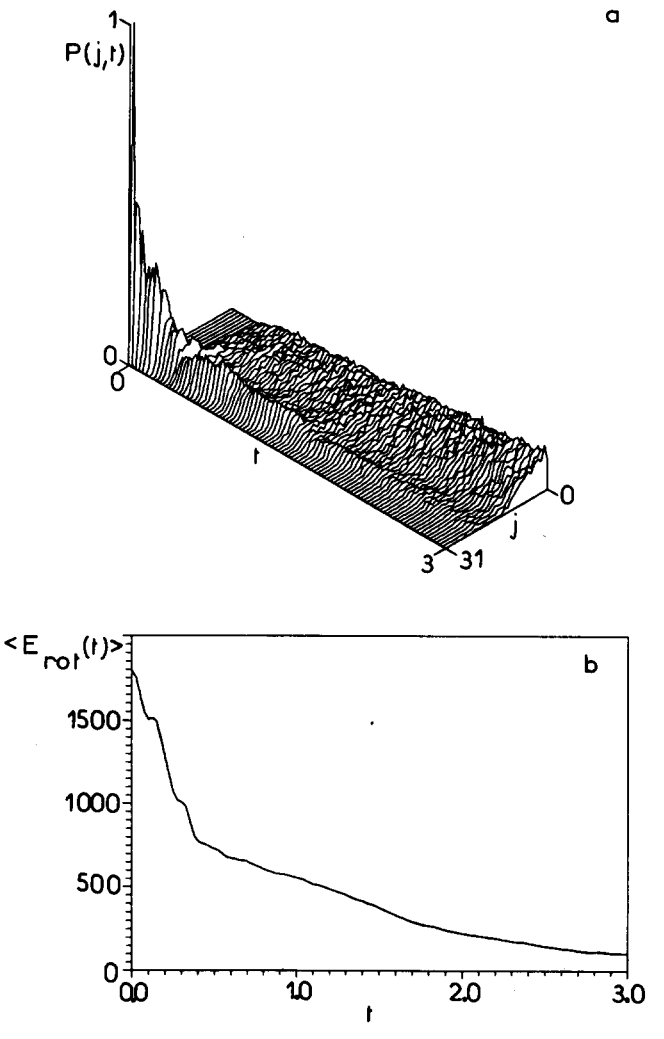

FIG. 9. Rotational energy relaxation for CO trapped in xenon crystal (the same as Fig. 3).

C. Xenon crystal

In xenon crystal, the existence of two different relaxation channels already mentioned in krypton appears clearly [cf. Figs. 9(a) and 9(b)]. The probability distribution function $P(j,t)$ is very broadened and 4 ps are necessary for this distribution to recover its equilibrium shape. All j values in the range (0–20) are highly probable, whereas higher values of j have a vanishing probability for $t \geqslant 0.4$ ps. This means that a rotational energy of about 500 cm^{-1} can be easily dissipated at short time, but much longer times are required to relax the remaining 1500 cm^{-1}.

Moreover, the relaxation rate of the total mean energy of the system (Fig. 10) becomes smaller and the probability distribution function $P(E,t)$ is obviously wider. Similar conclusions can be done on the functions $P(E_{c.m.},t)$ and $P(E_{at},t)$ [cf. Figs. 11(a) and 11(b)] which considerably broaden. The curves of mean energies $\langle E_{c.m.}(t)\rangle$ and $\langle E_{at}(t)\rangle$ still exhibit peaks with energies equal to 300 cm^{-1} at short time ($t \leqslant 1$ ps), but they remain nearly constant (around 200 cm^{-1}) over a long time scale, as a consequence of the inefficiency of the relaxation mechanisms. Note also that a feedback effect between the various modes could possibly explain these results (cf. Sec. V). In that case, the energy of the primary system could be transferred back to the molecule rotation, directly or via the local mode.

To conclude this section, striking environmental effects occur by changing the rare gas species. The relaxation mechanism which seems to be dominated by the local mode chan-

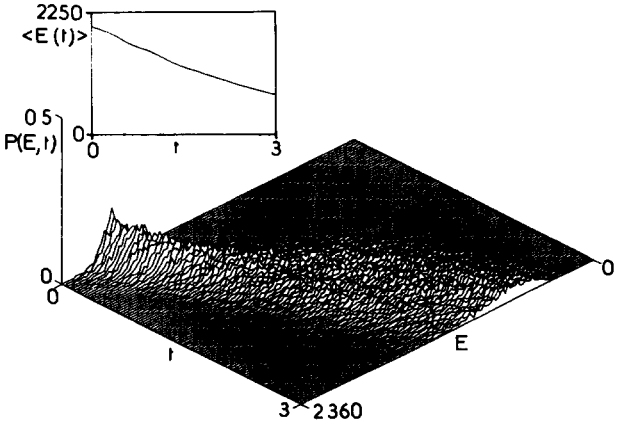

FIG. 10. Energy of the system "molecule-primary system" for CO trapped in xenon (the same as Fig. 4).

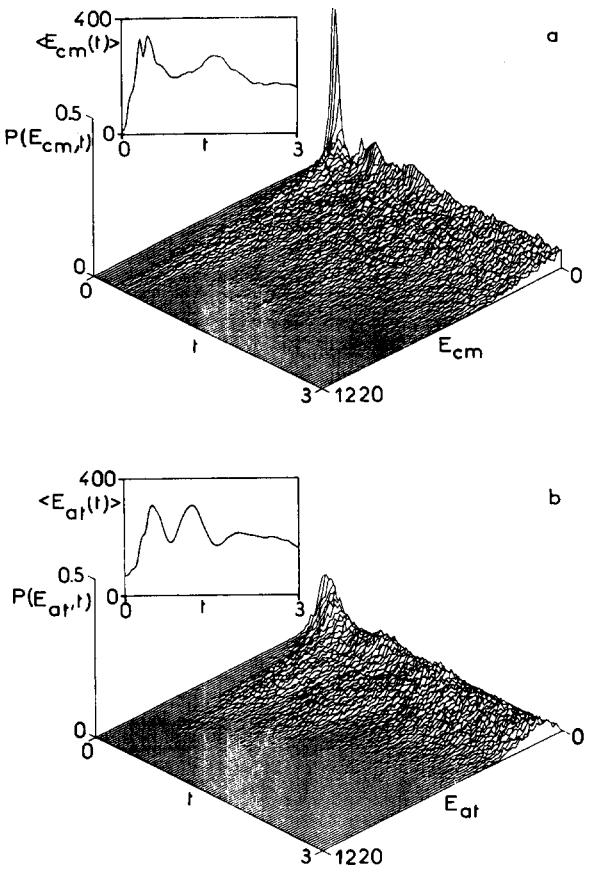

FIG. 11. Rotational relaxation for CO trapped in xenon crystal. (a) Energy (cm^{-1}) of the local translational mode vs time (ps); (b) energy (cm^{-1}) of the primary system modes vs time (ps).

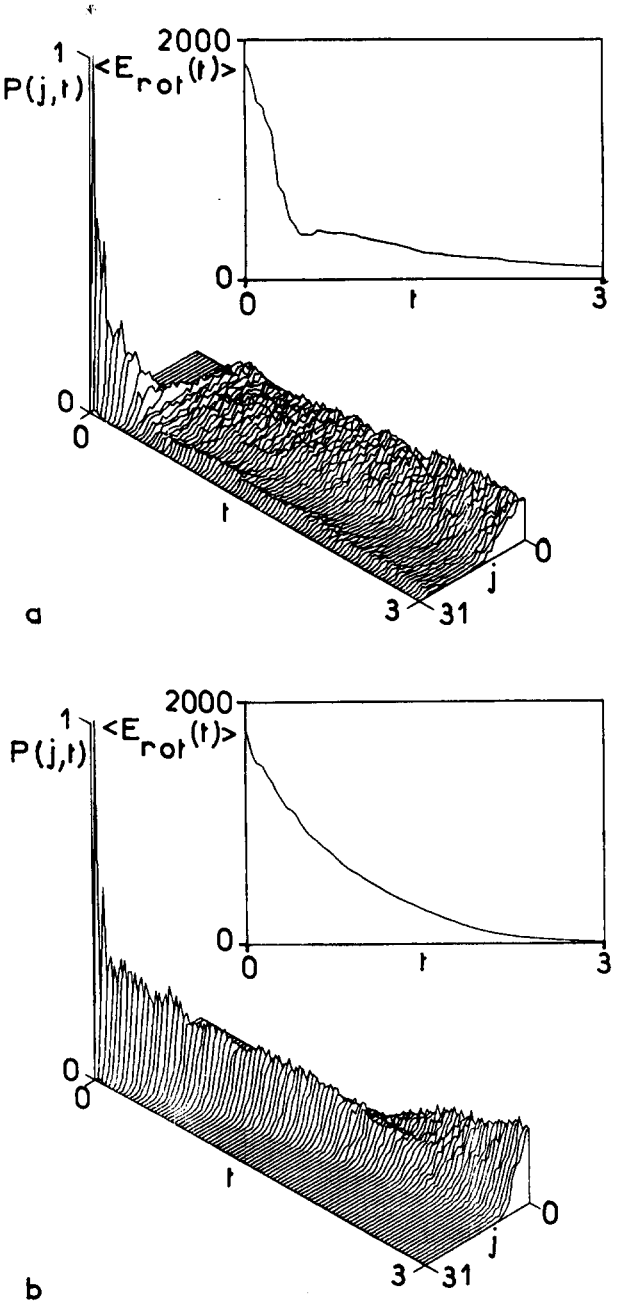

FIG. 12. Rotational relaxation for CO trapped in argon crystal. (a) The probability distribution function $P(j,t)$ and mean rotational energy $\langle E_{\rm rot}(t)\rangle$ when the only relaxational channel is the local mode; (b) the same curves when the direct relaxational channel only is considered.

nel in the lighter rare gas crystal exhibits a trend for a superimposition of two channels as the mass of the rare gas atom increases. The interpretation of the relaxational mechanisms is yet not straightforward on the basis of these results. Indeed, Figs. 3–11 do not give direct information on the energy quantity accepted by each mode, but instead, they represent only the difference between the stored and the released energy at each time. Moreover, the dynamical coupling between all the modes does not allow us to determine unambiguously the most efficient relaxational channel. Finally, it is not possible to calculate the part of the rotational energy which is directly transferred to the bulk crystal. All these points require a further separation of the relaxation channels, as shown in Fig. 1.

V. THE ROTATIONAL RELAXATION CHANNELS

In this section, we analyze the relative contributions of the molecular local mode and of the crystal modes in the rotational relaxation mechanism by considering these two channels in a separate way [cf. Figs. 1(b) and 1(c)].

A. Argon crystal

Figures 12(a) and 12(b) exhibit the probability distribution functions $P(j,t)$ when the rotational energy dissipation proceeds via the local mode channel only or directly towards the crystal modes. The behavior with time of the corresponding rotational energy is given for the two cases. These curves may be compared to the curves obtained in the general case (Fig. 3). We see that, at short time $t \leqslant 0.5$ ps, the distribution in Fig. 12(a) is very similar to the general one. However, for longer times, the first distribution becomes wider than the second; this indicates a lesser dissipation efficiency. As already mentioned, this could be partly due to the numerical trick used to isolate the primary system from the other relaxational modes which prevents energy transfer from the local mode to the primary system. This leads to a feedback mechanism for which the local mode is unable to dissipate more energy and it gives back a part of this energy excess to the molecular rotation. Such a phenomenon is ex-

hibited by the noticeable probability for finding high j values at long times [Fig. 12(a)] and by the behavior with time of the mean rotational energy. After a rather rapid decrease of this latter energy for $t \leqslant 0.4$ ps, very similar to the behavior observed in the general case [Fig. 3(b)], the slope of the curve suddenly decreases; the energy excess (about 400 cm^{-1}) can no longer be dissipated and the local mode saturates.

The probability distribution function $P(j,t)$ corresponding to the contribution of the crystal modes only [Fig. 12(b)] exhibits a monotonously slow decrease of the rotational quantum number j. The slight increase of the relaxation rate, around 2 ps, corresponds to a resonance between the rotational and the crystal modes. The exponential decreasing time behavior of the mean rotational energy with a large time constant characterizes a relaxation process which follows a first-order rate law. It is obvious that the curves of Fig. 12(b) do not exhibit the behavior of the general curves (Fig. 3), at least at short times.

From these results, we can thus conclude that the relaxation of the rotational molecular energy in argon crystal is mainly due to the local translational mode of the molecule which acts as an efficient energy acceptor. In fact this efficiency is probably underestimated in our results since, as mentioned before, we have disregarded the coupling between this local mode and the primary system [Fig. 1(b)]. An optimal efficiency would lead to a less wide distribution shape for low values of j and to a saturation energy much smaller than the value observed in Fig. 12(a).

B. Krypton crystal

A similar analysis of the relative contribution of the two channels for the rotational relaxation of CO trapped in krypton crystal is presented in Figs. 13(a) (local mode channel) and 13(b) (crystal modes). Whereas the short time behavior of the probability distribution function $P(j,t)$ connected to the relaxation via the local mode is similar to the general case [Fig. 6(a)], as for argon crystal, the long time evolution ($t \geqslant 0.3$ ps) exhibits very striking damped oscillations. These oscillations of the distribution function characterize the successive transfers of the energy from the local mode to the rotation and vice versa. The small damping with a large time constant and the sharp shape of the distribution around high j values show that the local mode is a very inefficient energy dissipator. This is particularly well shown on the curve $\langle E_{\rm rot}(t) \rangle$, where, after 0.3 ps, the mean rotational energy remains nearly constant around a value equal to 1250 cm^{-1}.

The crystal modes in krypton crystal are as in argon very inefficient energy dissipators [Fig. 13(b)]. This is clearly shown in the curve $\langle E_{\rm rot}(t) \rangle$ where the exponential time behavior with a large time constant is very similar to that drawn for argon crystal. However, since the local mode channel is also inoperant as a dissipator, both channels appear to play a more similar role in the rotational energy relaxation. The simultaneous analysis of Figs. 6 and 13 allow us to understand the occurrence, in the general case (Fig. 6) of a second probability line due to the influence of the crystal modes in the relaxation mechanism.

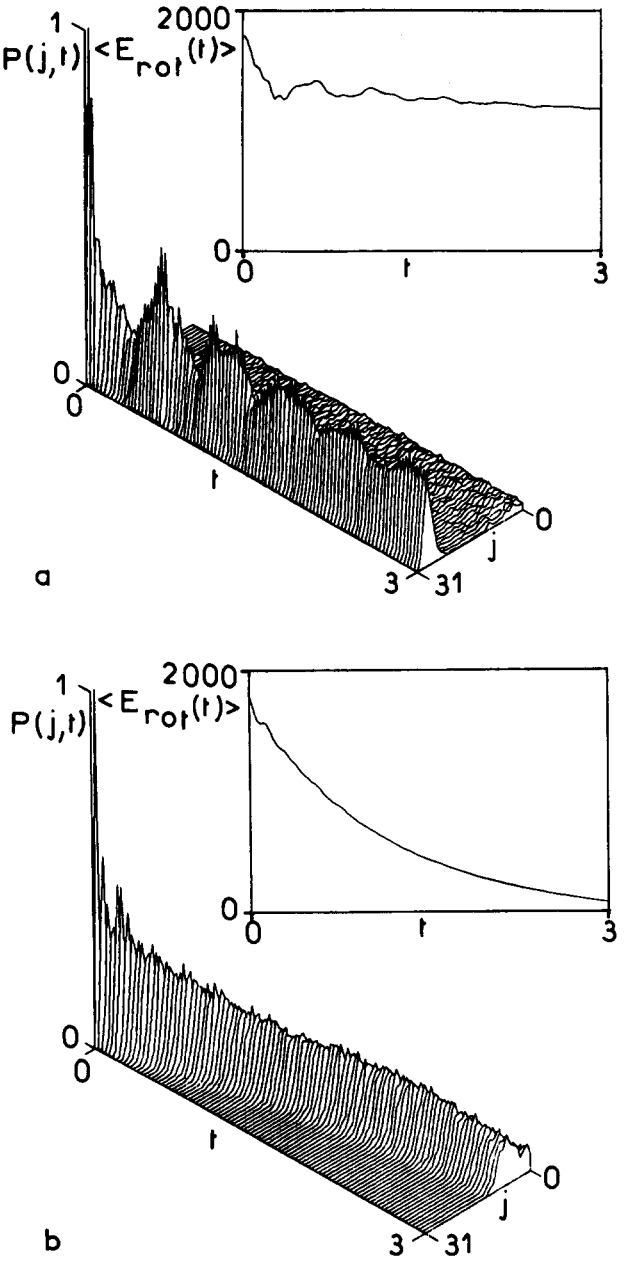

FIG. 13. CO trapped in Kr crystal (the same as Fig. 12).

The comparison of curves $P(j,t)$ and $\langle E_{\rm rot}(t) \rangle$ of Figs. 6 and 13 at short times ($t \leqslant 0.3$ ps) also shows that the initial acceptor of rotational energy is the local translational mode. This was not at all obvious from the single analysis of the energy curves obtained for the general case. The large initial slope of the curve $\langle E_{\rm rot}(t) \rangle$ in Fig. 13(a) exhibits in fact a break which is probably too energetic. Indeed the already mentioned numerical trick is responsible for a decrease of the dissipation efficiency of the local mode. Therefore, if the dynamical coupling between the local mode and the primary system did not vanish, we would expect a curve $\langle E_{\rm rot}(t) \rangle$ with a less energetic asymptote in the range 1–3 ps.

We can thus conclude that the rotational relaxation of CO in krypton crystal is a superimposition of two processes. The local mode is the first energy acceptor, but the crystal mode relaxation channel becomes more and more important as time increases. This second channel appears in fact domi-

nant at long times due to the inability of the local mode to dissipate the energy excess.

C. Xenon crystal

The stochastic classical trajectory results in the heaviest rare gas crystal are presented in Fig. 14. The same features as for krypton, but even magnified, are obtained with xenon. The damped oscillations of $P(j,t)$ connected to the contribution of the local mode only in the relaxation process characterize the dissipation unefficiency of this channel [Fig. 14(a)]. On the other hand, the crystal modes appear to be very poor energy dissipators with respect to the krypton case since the distribution function [Fig. 14(b)] remains narrow and concentrated around high j values even at $t \simeq 3$ ps. The curve $\langle E_{\rm rot}(t) \rangle$ for the local mode is nearly constant, after a rapid decrease at short time, whereas the same curve for the crystal modes monotonously decreases with a very large time constant.

Thus in the heaviest crystal, there is a striking separation between the relaxation channels. At short times, the rotational energy is dissipated via the local mode channel and the direct relaxation on the bulk crystal is negligible. At long times, the crystal mode channel supplements the local mode one and becomes the single energy acceptor. Figure 9 exhibits clearly this separation with the occurrence of two different probability lines. Of course, the fact that the distribution in Fig. 9 is not a simple superimposition of the distribution obtained in Fig. 14(a) and 14(b) can be interpreted as the result of the influence of intermediate dynamical couplings between the local mode and the crystal motions. These couplings, which are switched off in cases b and c of Fig. 1, allow the energy to be shared among the various acceptors in the general case.

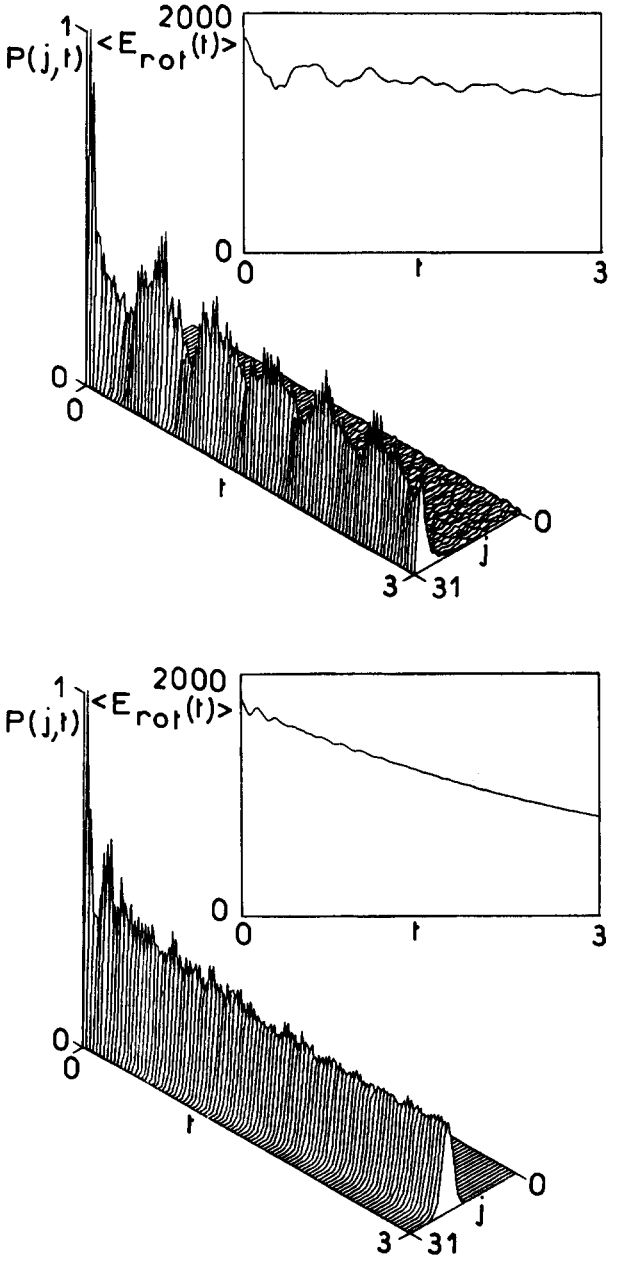

FIG. 14. CO trapped in Xe crystal (the same as Fig. 12).

VI. DISCUSSION

A. Interpretation of the results in terms of dynamical couplings

The results obtained in Secs. IV and V show that a CO molecule trapped in rare gas crystals at $T = 20$ K can relax large rotational energies ($j \simeq 30$) over the picosecond scale. The relaxation times increase in the sequence Ar, Kr, Xe. In fact, the relaxation processes in Kr and Xe are, respectively, three and eight times longer than in Ar crystal. At early times ($t \leqslant 0.5$ ps), the local translational mode of the impurity appears as the dominant relaxation channel, being responsible for the relaxation of 95%, 75%, and 60% of the rotational energy excess in Ar, Kr and Xe crystals, respectively. The remaining energy is then dissipated over longer times, mainly via the crystal modes.

Two species of quantities change when a rare gas is substituted to another one—the atom mass and the dynamic couplings. Both occur in the friction coefficients β_ϵ through the T_ϵ tensors [Eq. (3)] and through the parameters Ω and Γ, which are directly connected to the Debye frequencies of the rare gas crystals. On the one hand, the relative masses of rare gas atoms with respect to the molecule are, respectively,

$$m_x = \frac{M_x}{M_0} = 1.4,\ 3{,}0,\ \text{and}\ 4.7, \quad \text{for X} = \text{Ar, Kr, and Xe.}$$

On the other hand, the ratio of the dynamic coupling force constants (T_ϵ) are, respectively,

$$r_x = 0.64,\ 0.30,\ \text{and}\ 0.05$$

and the corresponding Debye frequencies are given in Table II.

So, when we compare the values of β_0 which characterizes the dissipative efficiency of the local mode, the ratio product $m_x \cdot r_x$ takes similar values for Ar and Kr, but it is about 4 times smaller for Xe. Moreover, the additional fact that the Debye frequency decreases as the rare gas atom mass increases leads to values of β_0 which follow the rule

$$\beta_0(\text{Ar}) > \beta_0(\text{Kr}) \gg \beta_0(\text{Xe}).$$

This rule explains why the local translational mode of the

molecule plays a much more significant role as an energy dissipator in Ar than in Kr and *a fortiori* in Xe crystal.

B. Application to other systems

On the basis of this simple discussion, we can wonder whether the present method could be applied to another physical systems. Applicability of the method rests on the following requirements:

(i) small rotational constant for the diatomic rotor in order to satisfy the validity condition of the classical treatment;

(ii) molecular rotation described by a single degree of freedom (planar rotation assumption);

(iii) molecular size consistent with a monosubstitutional crystal site;

(iv) assumption of Markovian dynamics valid for most of the crystal shells, including part of the first shell.

Hydrogenated diatomic molecules which are generally potential candidates to vibrational relaxation mechanisms via the rotational modes do not satisfy requirements (i) and (ii). On an other hand, vibrationally excited molecules such as CO or N_2 are known to relax energy excess by a radiative process via migration in the crystal. Larger diatomics, such as halogenures, which could relax via local mode and/or multiphonon channels do not necessarily verify item (iii). Thus, it appears that the molecular system considered in this paper can be considered rather as a model system for polyatomic molecules undergoing specific motions in crystals. For instance, CH_3F would be an interesting candidate for simulation calculations in the sense that it can be schematized as a diatomic (CH_3–F) rotor which undergoes in rare gas matrices hindered quasi-2D rotational motions.[10] Without releasing requirements (i) and (ii), we can yet say that the third item appears less compelling and consider also the motions of parts of large polyatomic molecules. Indeed, for these latter species, rotamerization phenomena induced by infrared laser excitations[17] take place in rare gas crystals. The rotation is typically described, in this case, by a single degree of freedom with relaxations governed by the surrounding crystal. The solid environment could be roughly represented by a limited number of effective atoms, which interact predominantly with the rotating part of the molecule. Simulation calculations on these larger systems for which quantum mechanical methods are untractable would probably provide useful semiquantitative informations on the relaxation mechanisms.

ACKNOWLEDGMENTS

A partial support from the Gobierno Autonomo de Canarias in the numerical part is greatly acknowledged.

[1] F. Legay, in *Chemical and Biological Applications of Lasers*, edited by C. B. Moore (Academic, New York, 1977); L. E. Brus and V. E. Bondibey, in *Radiationless Transitions*, edited by S. H. Lin (Academic, New York, 1980).

[2] H. Dubost, A. Lecuyer, and R. Charneau, Chem. Phys. Lett. **66**, 191 (1979); V. E. Bondibey, J. Chem. Phys. **65**, 5138 (1976); J. M. Wiesenfeld and C. B. Moore, *ibid.* **70**, 930 (1979); M. Allavena, H. Chakroun, and D. White, *ibid.* **77**, 1757 (1982); and previous references quoted in these papers.

[3] P. Boissel, B. Gauthier-Roy, and L. Abouaf-Marguin, J. Chem. Phys. **82**, 1056 (1985); L. Abouaf-Marguin and B. Gauthier-Roy, Chem. Phys. **51**, 213 (1980); L. Young and L. B. Moore, J. Chem. Phys. **76**, 5869 (1982); L. H. Jones and B. I. Swanson, *ibid.* **76**, 1634 (1982); V. A. Apkarian and E. Weitz, *ibid.* **76**, 5796 (1982); and previous references quoted in these papers.

[4] A. Nitzan and J. Jortner, Mol. Phys. **23**, 713 (1973); A. Nitzan, S. Mukamel, and J. Jortner, J. Chem. Phys. **60**, 3929 (1974); **63**, 200 (1975); J. Jortner, Mol. Phys. **32**, 379 (1976).

[5] S. H. Lin, J. Chem. Phys. **61**, 3810 (1974); **65**, 1053 (1976); H. Kono and S. H. Lin, *ibid.* **78**, 2607 (1983); **79**, 2748 (1984).

[6] D. J. Diestler, J. Chem. Phys. **60**, 2692 (1974); Mol. Phys. **32**, 1091 (1976); D. J. Diestler, E. W. Knapp, and H. D. Ladouceur, J. Chem. Phys. **68**, 4056 (1978).

[7] K. F. Freed and H. Metiu, Chem. Phys. Lett. **48**, 262 (1977); **49**, 19 (1977).

[8] R. B. Gerber and M. Berkowitz, Chem. Phys. Lett. **49**, 260 (1977); Mol. Phys. **36**, 355 (1978).

[9] C. Girardet and A. Lakhlifi, J. Chem. Phys. **83**, 5506 (1985); **87**, 4559 (1987).

[10] A. Lakhlifi and C. Girardet, J. Chem. Phys. **90**, 1345 (1989).

[11] V. Delgado, J. Breton, and C. Girardet, J. Chem. Phys. **87**, 4802 (1987).

[12] V. Delgado, J. Breton, A. Hardisson, and C. Girardet, J. Chem. Phys. **87**, 4809 (1987).

[13] (a) M. Shugard, J. C. Tully, and A. Nitzan, J. Chem. Phys. **69**, 336 (1978); (b) **69**, 2525 (1978); (c) **78**, 3959 (1983).

[14] S. A. Adelman and J. D. Doll, J. Chem. Phys. **64**, 2375 (1976); S. A. Adelman, *ibid.* **71**, 4471 (1979); Adv. Chem. Phys. **44**, 143 (1983); J. Chem. Phys. **88**, 4397 (1988); **88**, 4415 (1988).

[15] C. L. Brookes III, M. W. Balk, and S. A. Adelman, J. Chem. Phys. **79**, 784 (1983); **79**, 804 (1983), and references quoted therein.

[16] $P(j,t)$ represents in fact $P(E_{\rm rot}(t))$ when the closest integer value of j, which verifies the identity $j(j+1) = E_{\rm rot}/B$, is replaced into P. This approximation is valid when B is small and $E_{\rm rot}$ is sufficiently large for the total rotational energy to be assimulated with the kinetic rotational energy of the diatomic molecule.

[17] J. Pourcin, G. Davidovics, H. Bodot, L. Abouaf-Marguin, and B. Gauthier-Roy, Chem. Phys. Lett. **74**, 147 (1980); S. Charbonnier, R. Viani, J. Pourcin, and H. Bodot, J. Mol. Structure **161**, 265 (1987).